Electronic Supporting Information

Exploring Coverage–Dependent Chain–Growth Mechanisms on Ru(111) for Fischer–Tropsch Synthesis

Yueyue Jiao[a,b,c], Huan Ma[a,b,c], Pengju Ren[a,c], Teng Li[d], Yong-Wang Li[a,b,c], Xiao-Dong Wen*[a,b,c,e], and Haijun Jiao*[f]

(a) State Key Laboratory of Coal Conversion, Institute of Coal Chemistry, Chinese Academy of Sciences, Taiyuan 030001, China. (b) The University of Chinese Academy of Sciences, Beijing 100049, China. (c) National Energy Center for Coal to Liquids, Synfuels China Co., Ltd., Beijing 101400, China. (d) State Key Laboratory for Oxo Synthesis and Selective Oxidation, Lanzhou Institute of Chemical Physics, Chinese Academy of Sciences, No.18, Tianshui Middle Road, Lanzhou, 730000, China. (e) Beijing Advanced Innovation Center for Materials Genome Engineering, Industry–University Cooperation Base between Beijing Information S&T University and Synfuels China Co. Ltd, Beijing, China. (f) Leibniz–Institut für Katalyse e.V.; Albert–Einstein Strasse 29a, 18059 Rostock, Germany: E–mails: wxd@sxicc.ac.cn; and Haijun.jiao@catalysis.de

As shown in Figure S1, there are merely consistent CO adsorption patterns on the Ru(0001) and Ru(111) surfaces. On Ru(111) (Figure S2), the first region shows a stable 1 ML CO coverage (9CO) from 0 to 225 K, where all adsorbed CO molecules are at the hcp sites (Figure S2). Very similar regions are found on Ru(0001). However, the 1 ML CO region is not found previously because of different model,[1] and the main difference comes from the adsorption sites (hcp vs. top). As shown in Table S1, the adsorption of all CO molecules at the hcp sites is 1.08 and 0.53 eV more stable than that at the top sites on the Ru(111) and Ru(0001) surfaces, respectively. Disordered CO adsorption on Ru(0001) was observed below 77 K by scanning tunneling microscopy (STM) in an ultrahigh vacuum (UHV) chamber with a base pressure of 7×10^{-11} mbar,[2] however, it does not give clear evidence about the CO coverage. Under UHV (5×10^{-11} mbar pressure), temperature programmed desorption (TPD) shows CO coverage of 0.54 ML at 370 K, 0.43 ML at 413 K and 0.22 ML at 490 K,[3] which is consistent with the computed results (dashed line, Figure S1b).

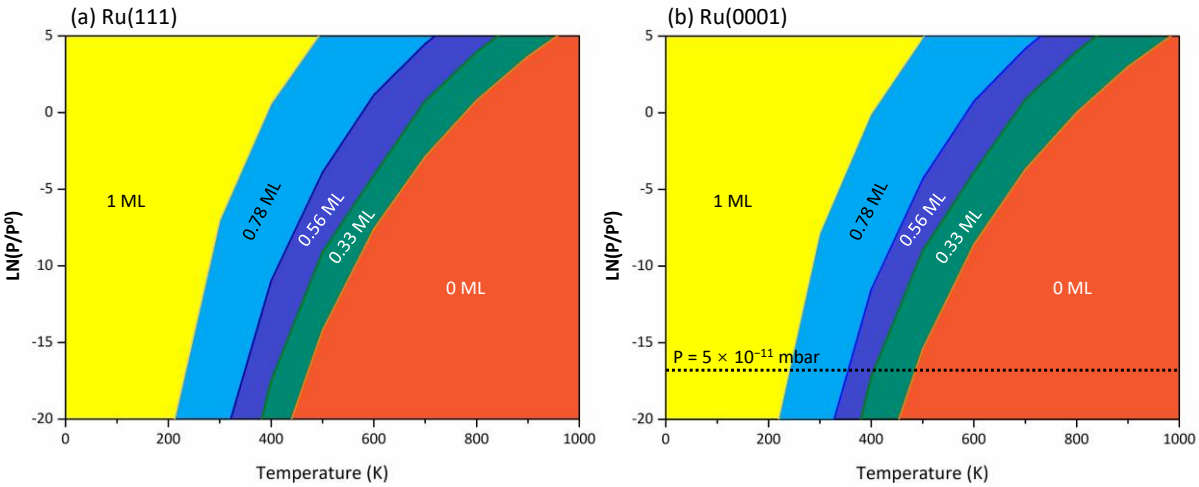

Figure S1. Phase diagrams of stable CO coverage as a function of temperature and CO partial pressure ($\ln(P/P^{\ominus})$). (a) Ru(111) surface (b) Ru(0001) surface (dash line for CO pressure of 5×10^{-11} mbar).

Table S1. DFT energies (E, eV) and zero-point energies (ZPE, eV) of 9 CO adsorbed at different sites on Ru(111) and Ru(0001).

	Ru(111)				Ru(0001)			
site	E	ZPE	E+ZPE	Δ(E+ZPE)	E	ZPE	E+ZPE	Δ(E+ZPE)
hcp	−434.30	1.95	−432.35	0.00	−436.94	1.92	−435.01	0.00
fcc	−433.78	1.92	−431.83	0.52	−436.73	1.99	−434.74	0.27
top	−433.35	2.10	−431.23	1.08	−436.67	2.12	−434.48	0.53
bridge	−433.75	2.04	−431.75	0.60	−436.60	2.00	−434.12	0.83

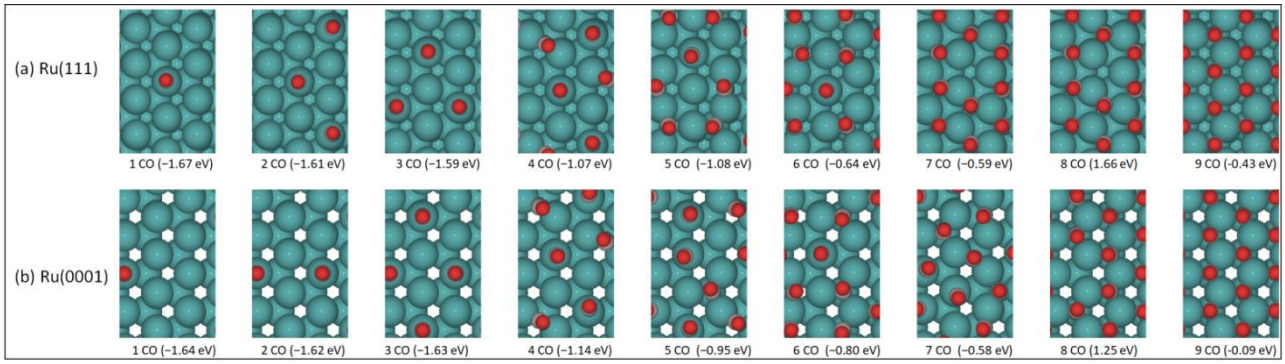

Figure S2. Stepwise adsorption energy (the values in the brackets) of CO. (a) Ru(111). (b) Ru(0001)

Table S2. Gibbs free energies (ΔG, eV) of the 1 H adsorption on the highest CO pre-covered Ru(111) surface and on the highest CO pre-covered Ru(111) surface with one CO desorption (423 K, 30 atm, and p_{H2}/p_{CO} = 2/1)

Reactions	ΔG
$7CO + 0.5H_2(g) = 7CO + H$	0.64
$7CO + 0.5H_2(g) = 6CO + H + CO(g)$	0.50

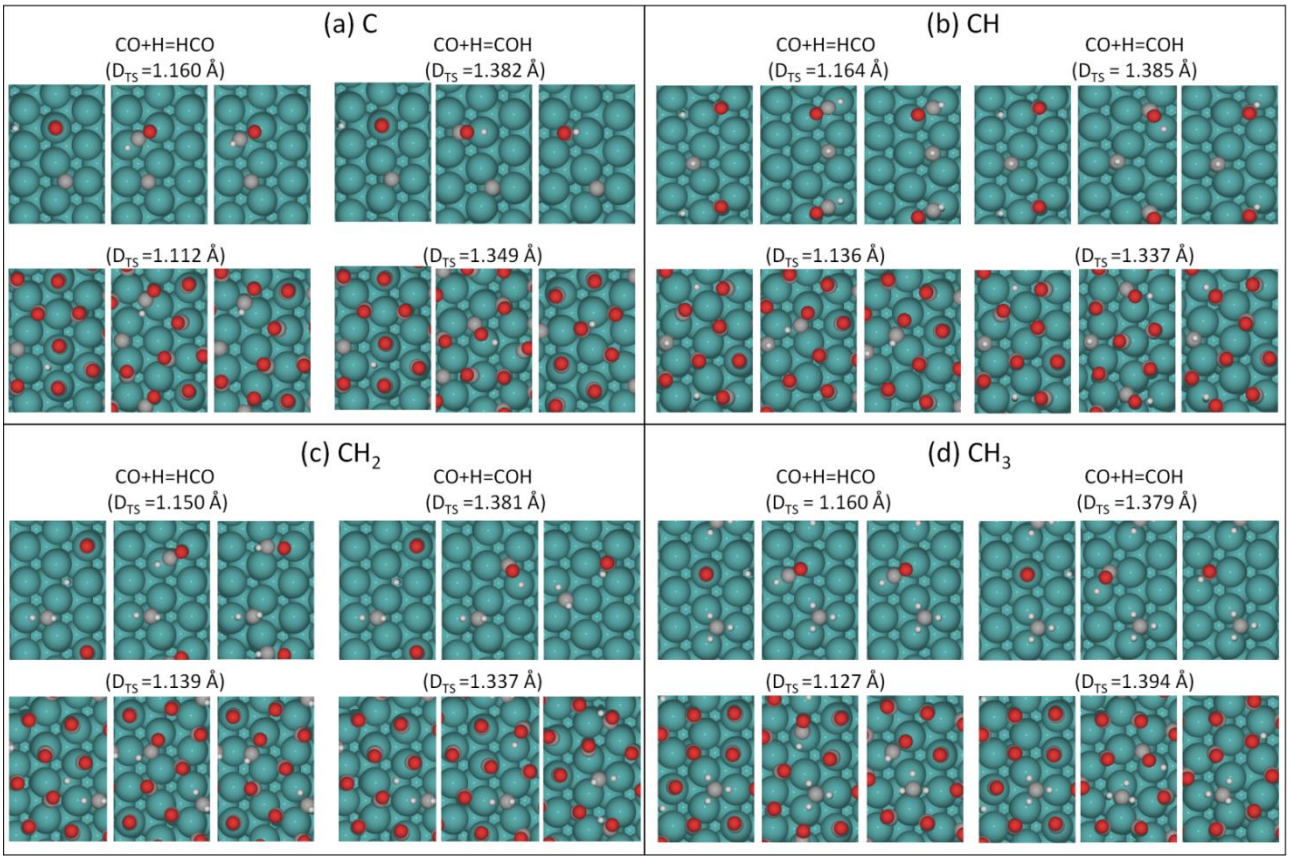

Figure S3. Surface structures of the initial (IS), transition (TS) and final (FS) states for the formation of HCO and COH on pre-adsorbed CH_x (x = 0-3) with the forming C-H bond length (D_{TS}) in the transition state (top structures are those at the lowest coverage, and bottom structures are those at CO pre-saturation coverage)

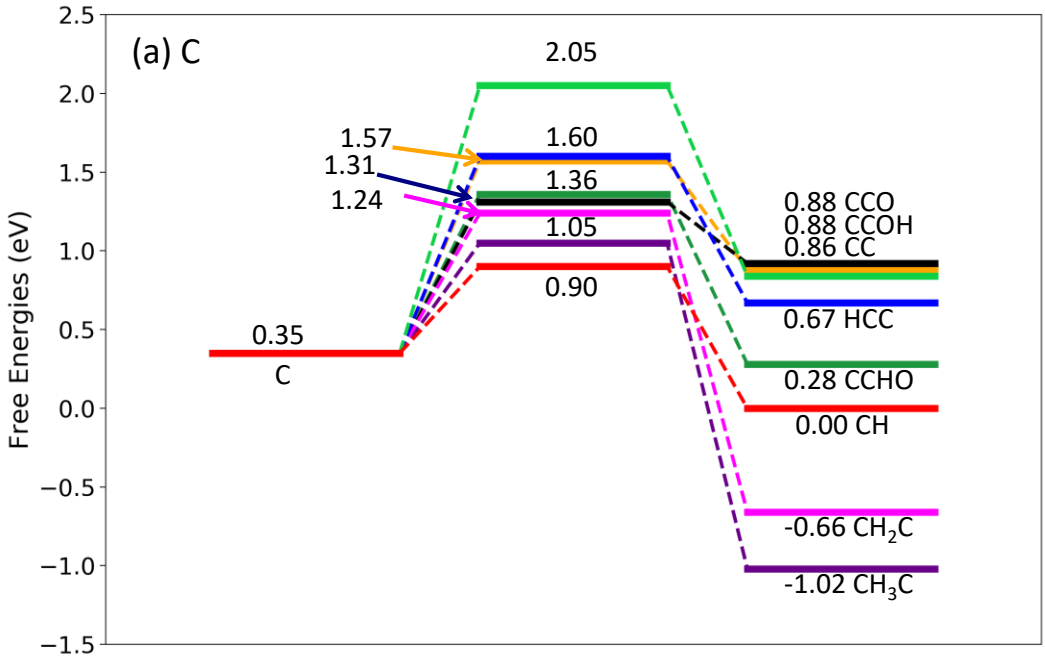

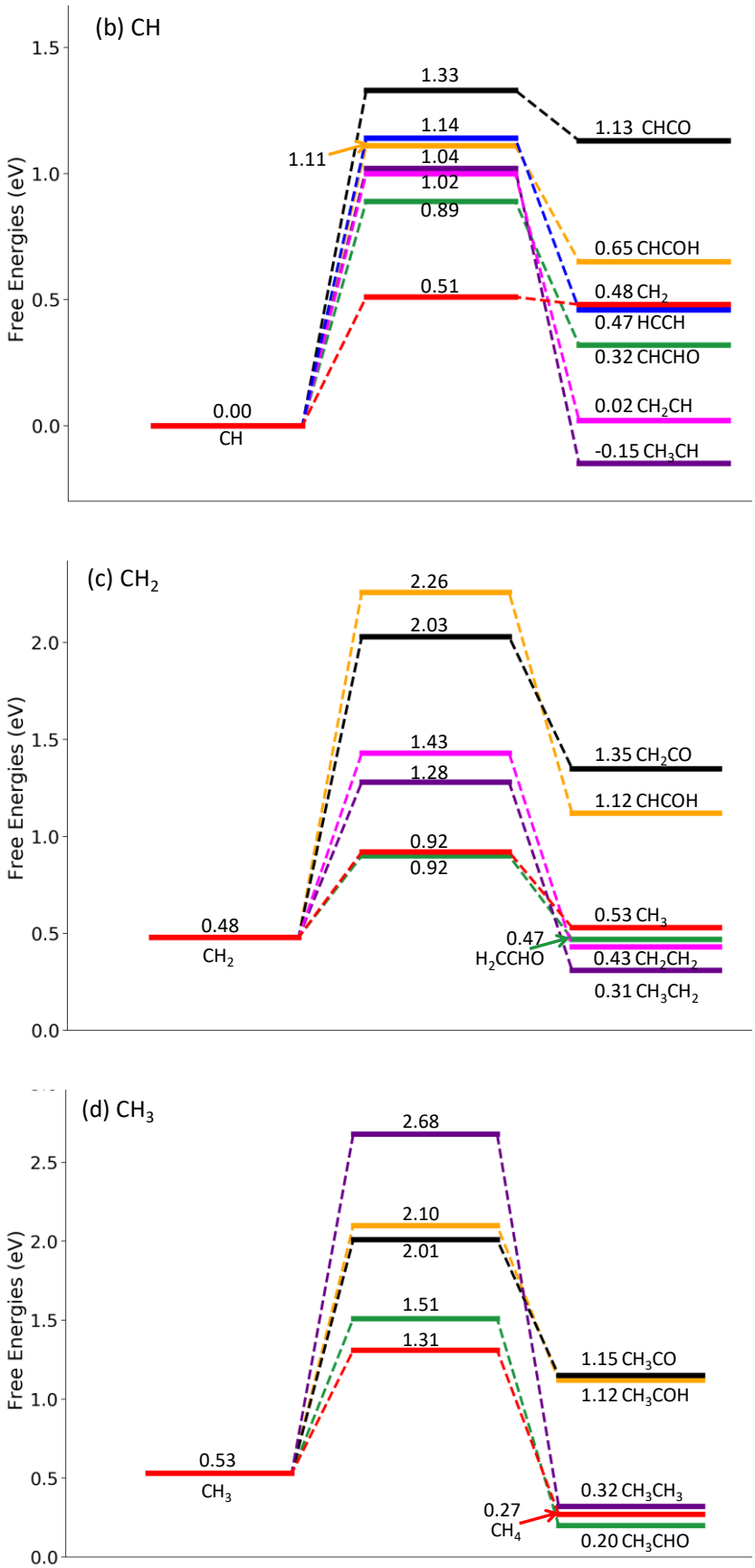

Figure S4. Gibbs free energy barriers and reaction energies (eV) for the competitive CH_x hydrogenation and CH_x-C1 coupling at the lowest coverage.

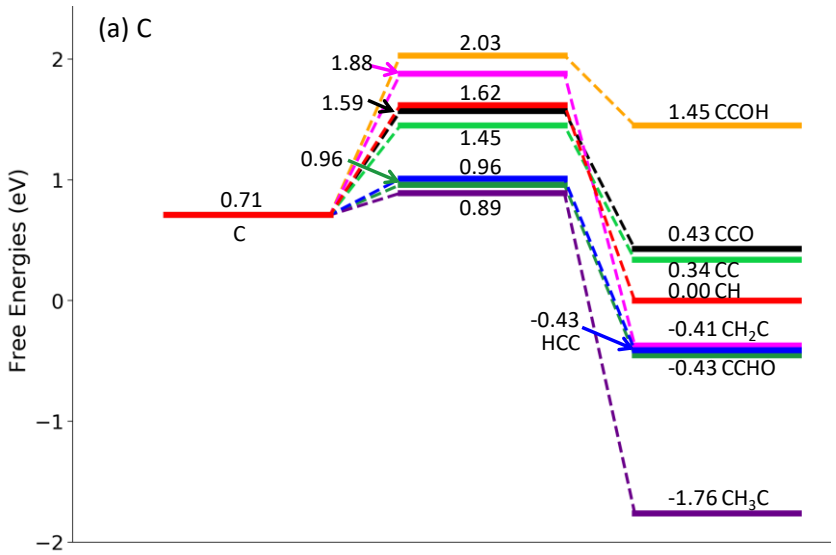
(a) C
Free Energies (eV)
2
1
0
−1
−2
0.71
C
1.88
1.59
0.96
2.03
1.62
1.45
0.96
0.89
1.45 CCOH
0.43 CCO
0.34 CC
0.00 CH
-0.41 CH2C
-0.43 CCHO
-0.43
HCC
-1.76 CH3C

1

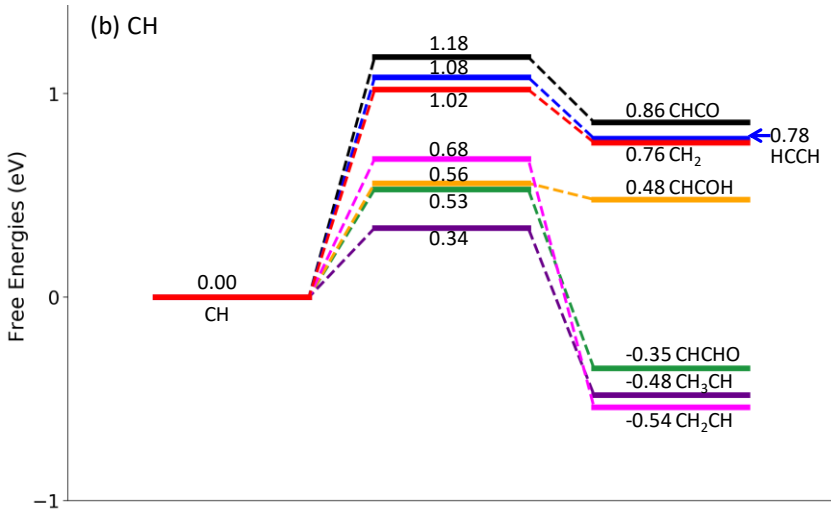
(b) CH
Free Energies (eV)
1
0
−1
0.00
CH
1.18
1.08
1.02
0.68
0.56
0.53
0.34
0.86 CHCO
0.78
HCCH
0.76 CH2
0.48 CHCOH
-0.35 CHCHO
-0.48 CH3CH
-0.54 CH2CH

2

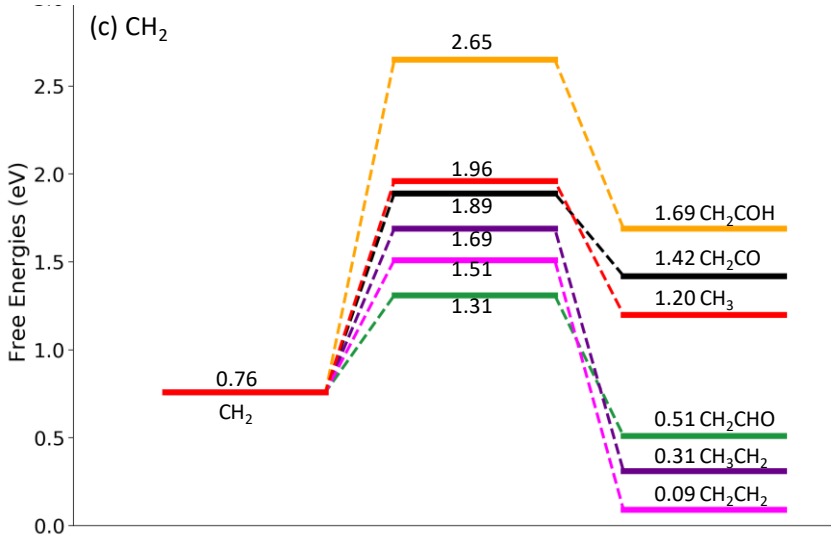
(c) CH2
Free Energies (eV)
2.5
2.0
1.5
1.0
0.5
0.0
0.76
CH2
2.65
1.96
1.89
1.69
1.51
1.31
1.69 CH2COH
1.42 CH2CO
1.20 CH3
0.51 CH2CHO
0.31 CH3CH2
0.09 CH2CH2

3

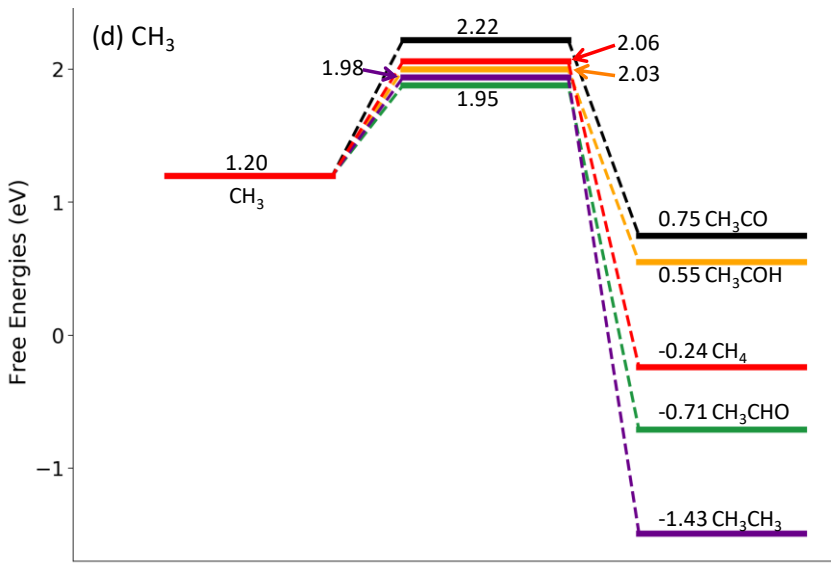

Figure S5. Gibbs free energy barriers and reaction energies (eV) for the competitive CH_x hydrogenation and CH_x-C1 coupling at CO pre-saturation coverage

Figure S6. Surface structures of the initial (IS), transition (TS) and final (FS) states for the competitive CH_x hydrogenation and CH_x-C1 coupling at the lowest coverage. Elementary reactions along with the forming C-H or C-C bond length (D_{TS}) in the transition states are given.

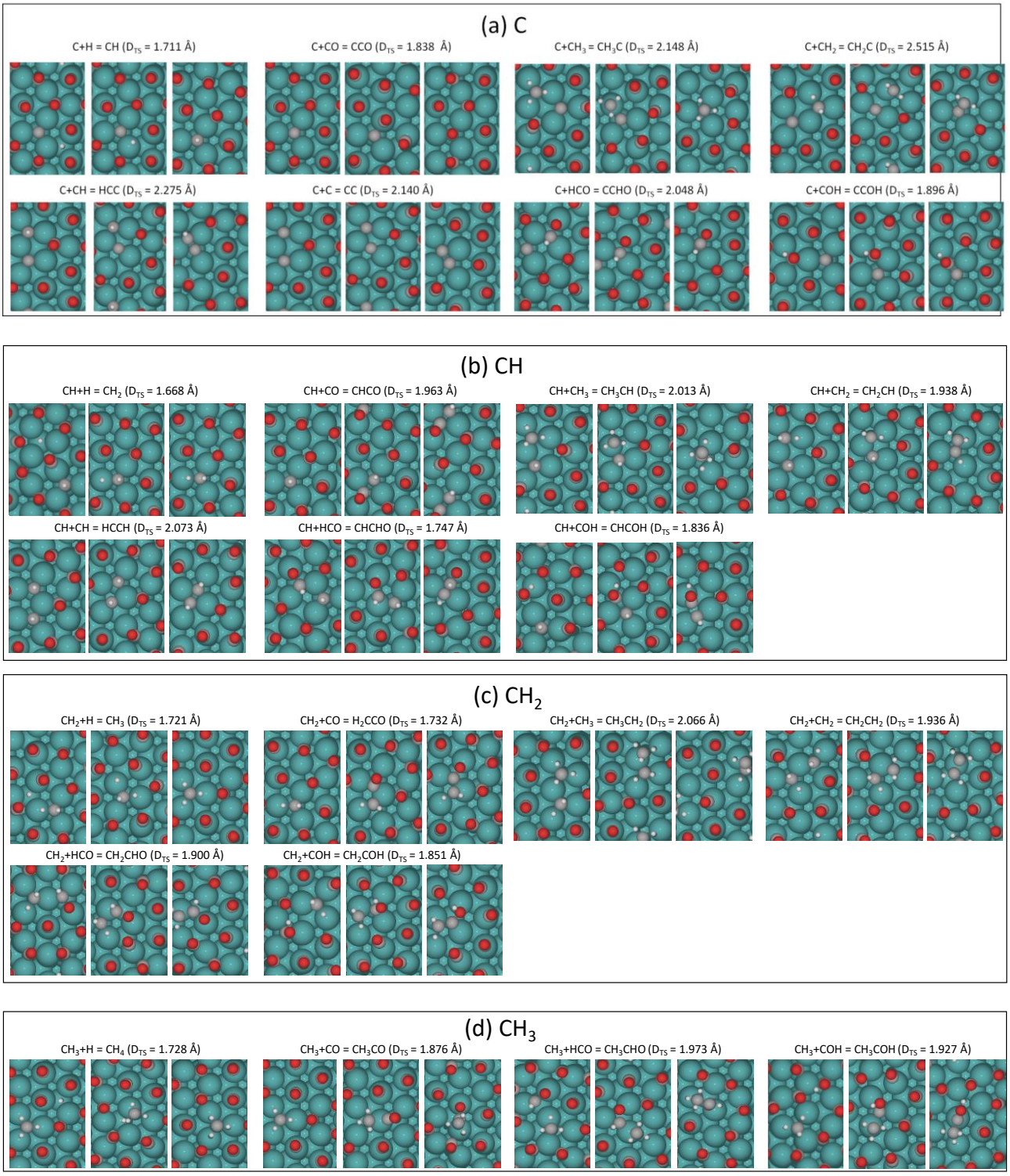

Figure S7. Surface structures of the initial (IS), transition (TS) and final (FS) states for the competitive CH_x hydrogenation and CH_x-C1 coupling at CO pre-saturation CO coverage. Elementary reactions along with the forming C-H or C-C bond length (D_{TS}) in the transition states are given.

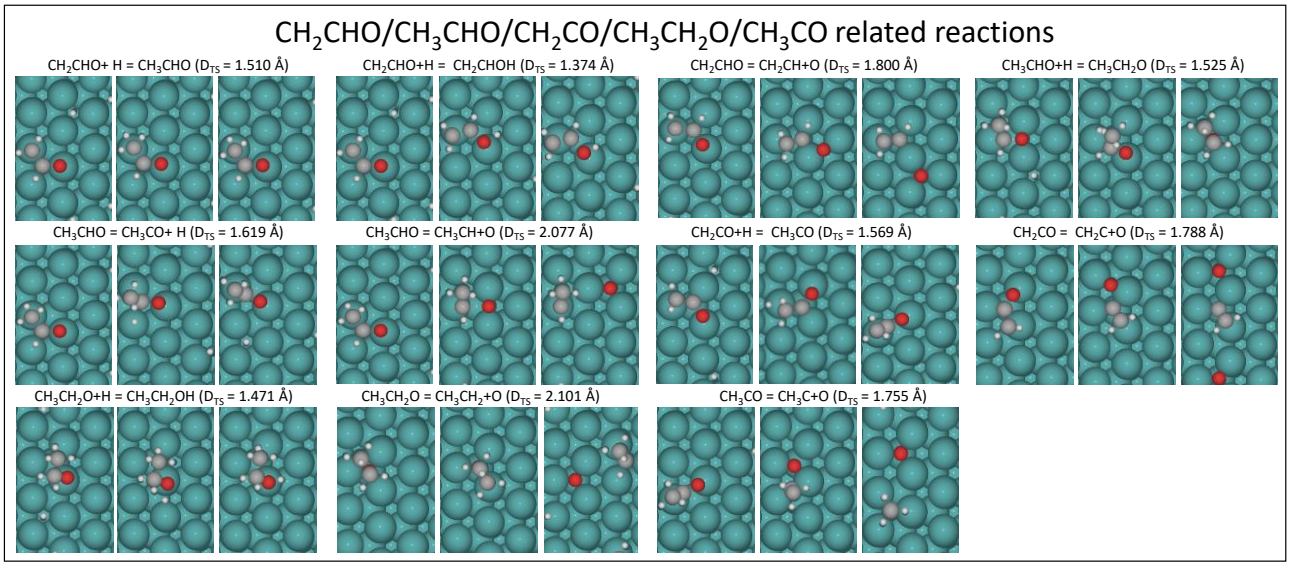

Figure S8. Surface structures of the initial (IS), transition (TS) and final (FS) states for $CH_2CHO/CH_3CHO/CH_2CO/CH_3CH_2O/CH_3CO$ related reactions at the lowest coverage. Elementary reactions along with the forming/dissociating C-X bond length (D_{TS}) in the transition states are given.

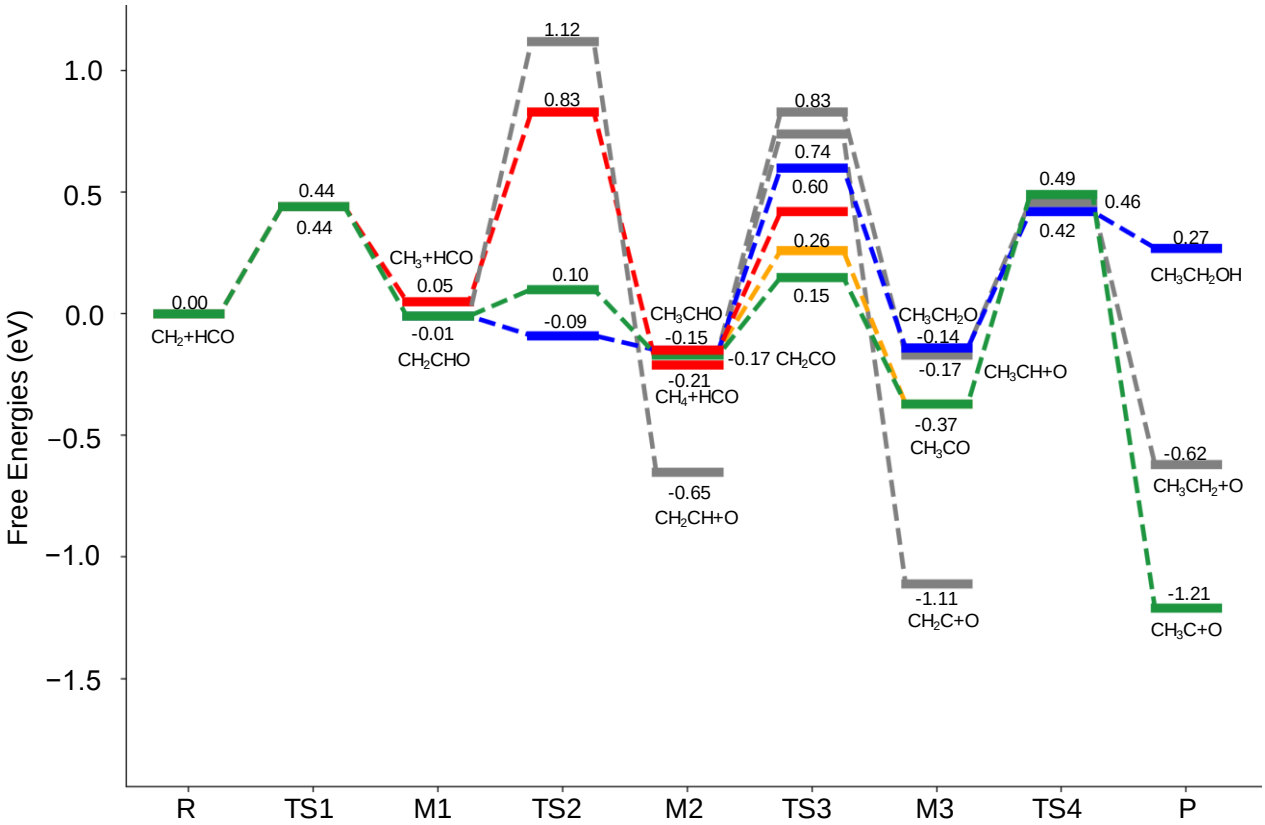

Figure S9. Gibbs free energy profiles of CH_2+HCO development on the basis of gaseous H_2 on Ru(111) at the lowest coverage

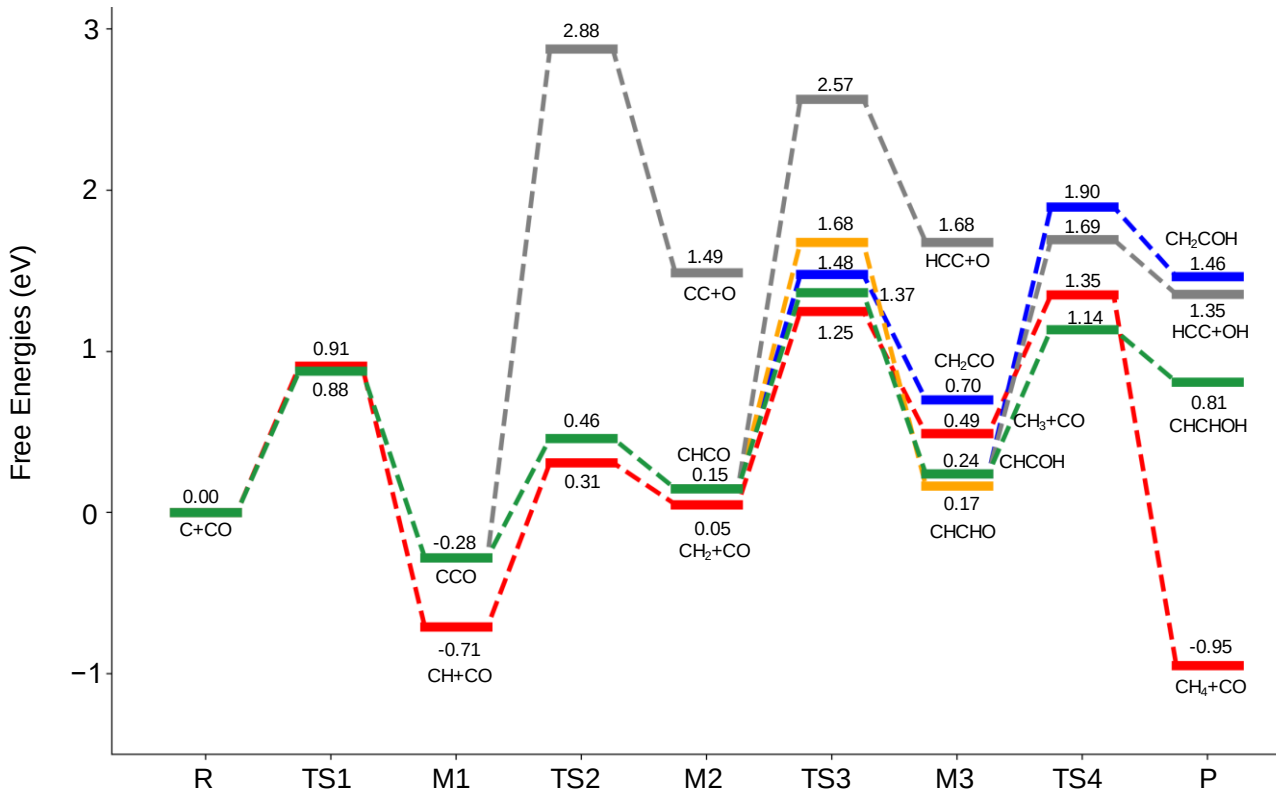

Figure S10. Gibbs free energy profiles of C+CO development on the basis of gaseous hydrogen at CO pre-saturation coverage

As shown in Figure S10, the coupling of C + CO, which has a barrier of 0.88 eV and is exergonic by 0.28 eV, is comparable kinetically with C + H reaction, although the coupling of C + CH_3, C + HCO, and C + CH has lower barrier and is more exergonic (0.18/−2.47 eV, 0.25/−1.14 eV, and 0.25/−1.14 eV, respectively, Figure S5a). Starting from CCO, CCO is more favored to be hydrogenated into CHCO, which has a barrier of 0.74 eV and is endergonic by 0.43 eV, while CCO dissociation into CC + O has a higher barrier (3.16 eV) and is much more endergonic (1.77 eV), due to its upright adsorption configuration. Afterwards, CHCO stepwise hydrogenation to CHCOH, CH_2CO, and CHCHO has barriers of 1.22, 1.33, and 1.53 eV and reaction free energies of 0.09, 0.55, and −0.02 eV, respectively, while CHCO dissociation into HCC + O has a barrier of 2.42 eV and is endergonic by 1.53 eV. The further hydrogenation of CHCOH to CHCHOH has a barrier of 0.90 eV and is endergonic by 0.57 eV. Combined with the results in Figure S5a, the barrier for the stepwise hydrogenation from C to CH_4 is 0.91, 1.02, 1.20, and 0.86 eV and the reaction free energy is −0.71, 0.76, 0.44, and −1.44 eV, respectively. Starting from C + CO, the most favored route is CH_4 formation, which has an apparent barrier of 1.35 eV and is exergonic by 1.05 eV, and the second most favored route is CCO → CHCO → CHCOH → CHCHOH, which has an apparent barrier of 1.37 eV and is endergonic by 0.81 eV. Thermodynamically, CH_4 formation at FTS initial reaction stage is much more favored. Along with the formation of CH_4, the first C2 initiator is produced on the surface.

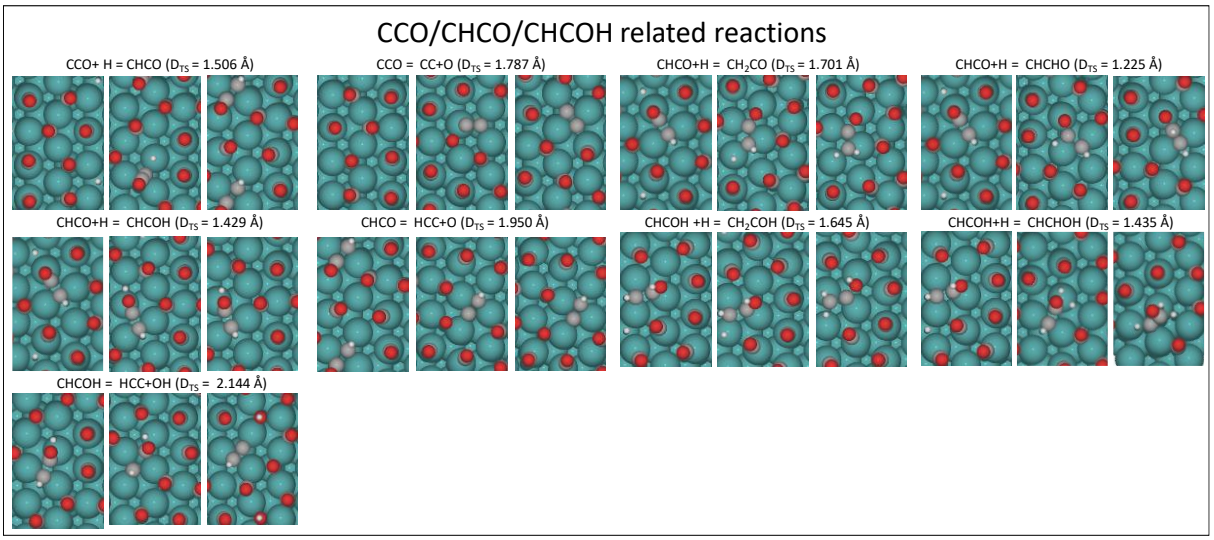

Figure S11. Surface structures of the initial (IS), transition (TS) and final (FS) states for the CCO/CHCO/CHCOH related reactions at CO pre-saturation coverage. Elementary reactions along with the forming/dissociating C-X bond length (D_{TS}) in the transition states are given.

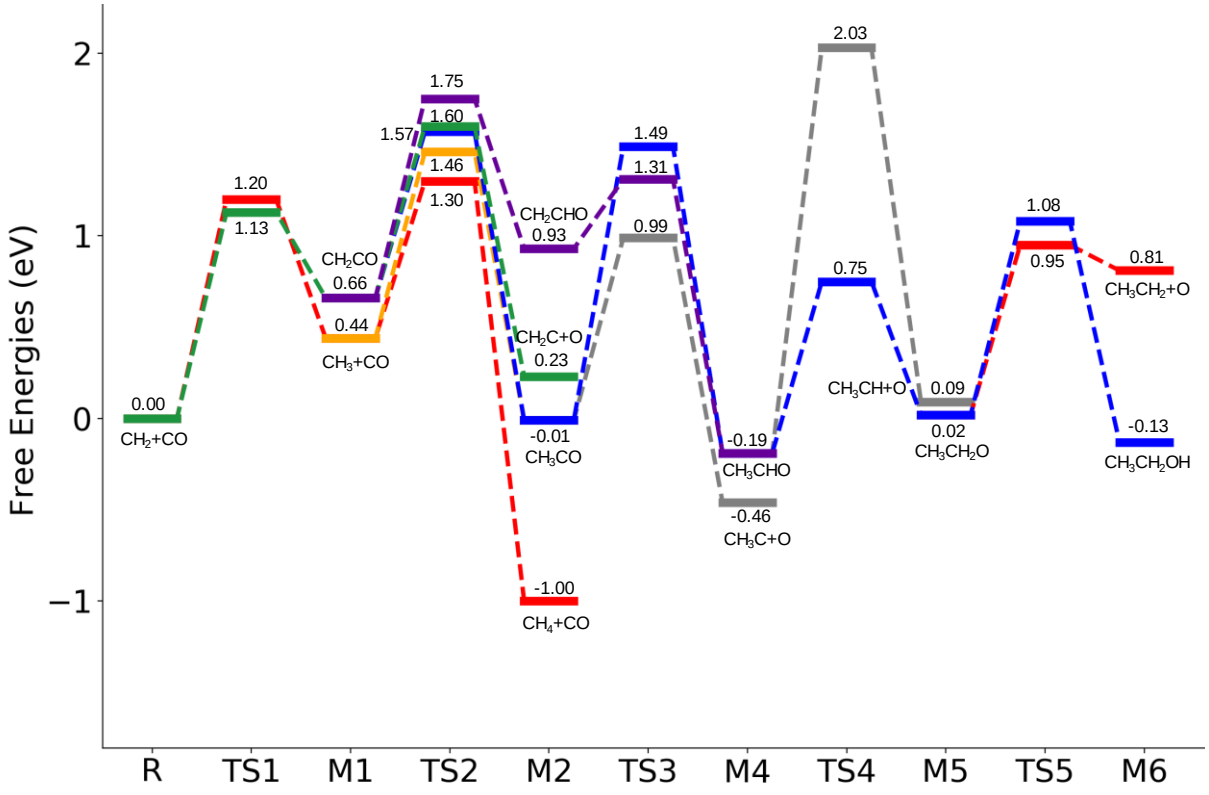

Figure S12. Gibbs free energy profiles of CH_2+CO development on the basis of gaseous hydrogen at CO pre-saturation coverage

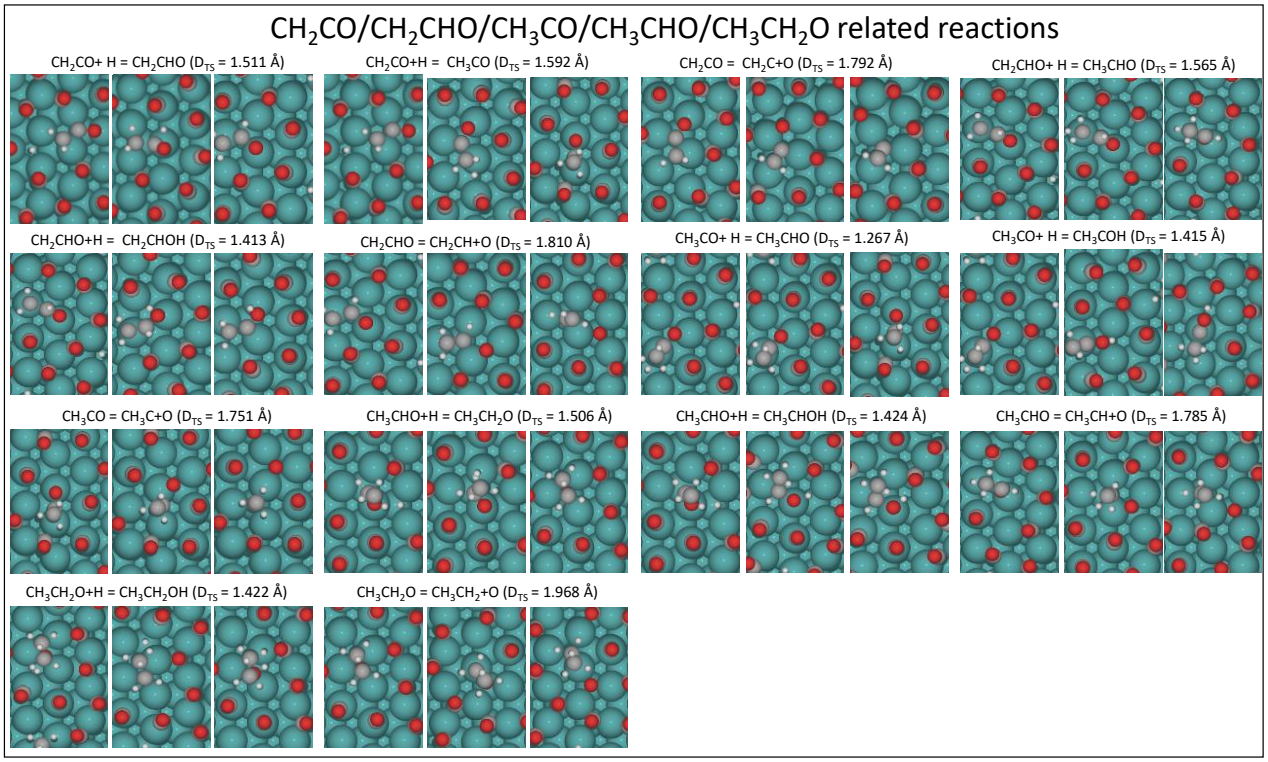

Figure S13. Surface structures of the initial (IS), transition (TS) and final (FS) states for the $CH_2CO/CH_2CHO/CH_3CHO/CH_3CH_2O$ related reactions at CO pre-saturation coverage. Elementary reactions along with the forming/dissociating C-X bond length (D_{TS}) in the transition states are given.

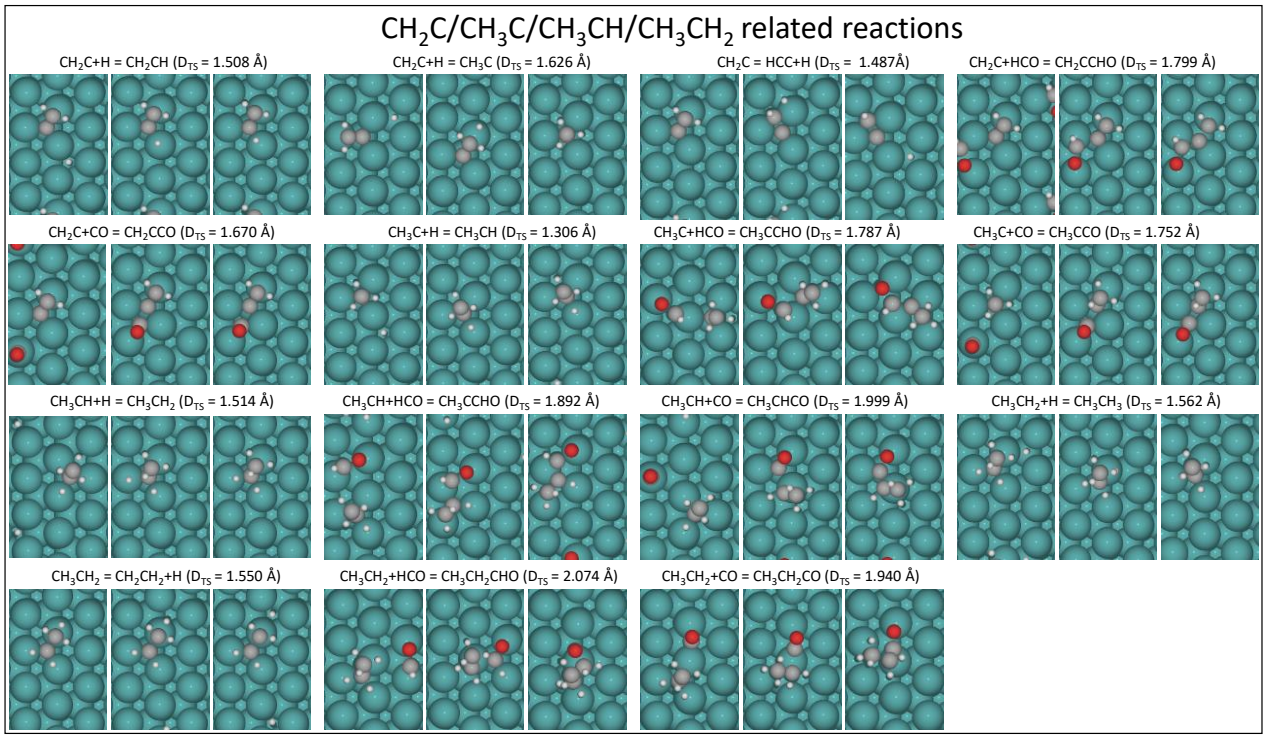

Figure S14. Surface structures of the initial (IS), transition (TS) and final (FS) states for the $CH_2C/CH_3C/CH_3CH/CH_3CH_2$ related reactions at the lowest coverage. Elementary reactions along with the forming/dissociating C-X bond length (D_{TS}) in the transition states are given.

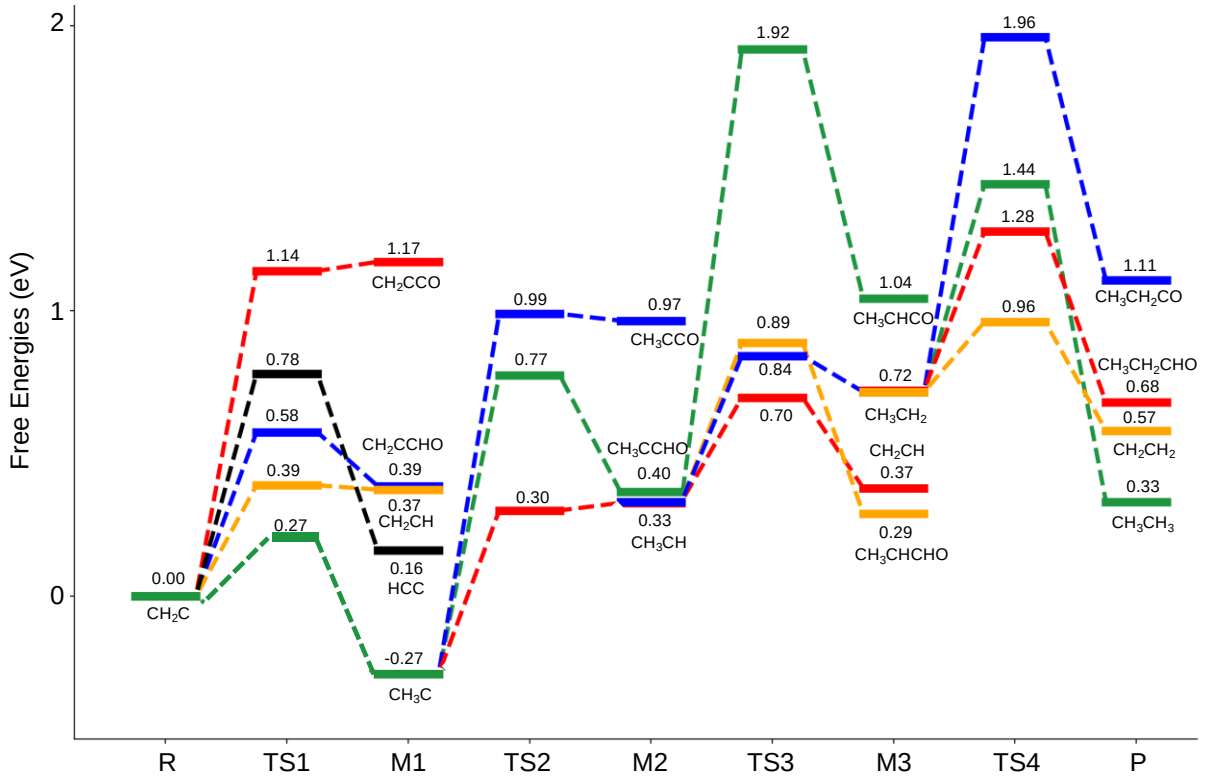

Figure S15. Gibbs free energy profiles of CH_2C development on the basis of gaseous hydrogen on Ru(111) at the lowest coverage. And the calculated CH_2CH related reactions

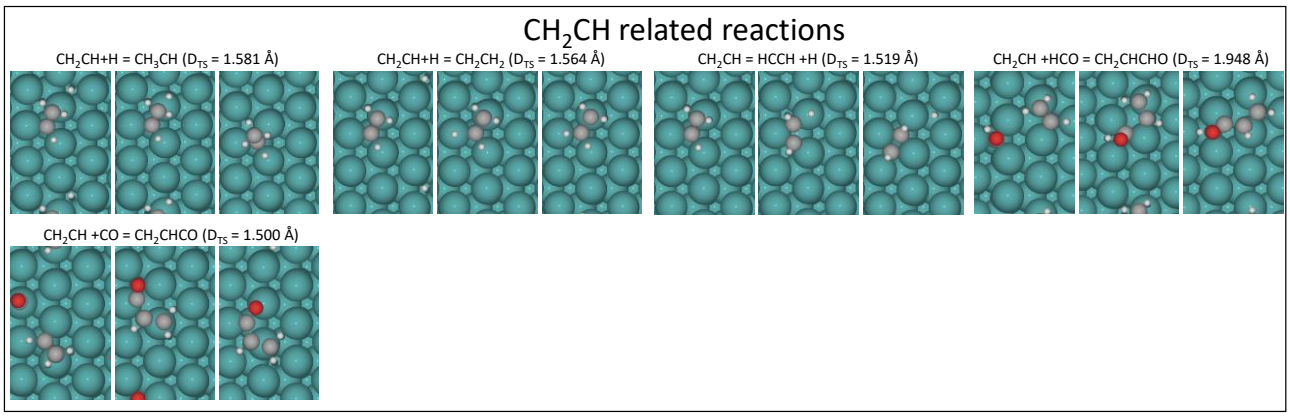

Figure S16. Surface structures of the initial (IS), transition (TS) and final (FS) states for the CH_2CH related reactions at the lowest coverage. Elementary reactions along with the forming/dissociating C-X bond length (D_{TS}) in the transition states are given.

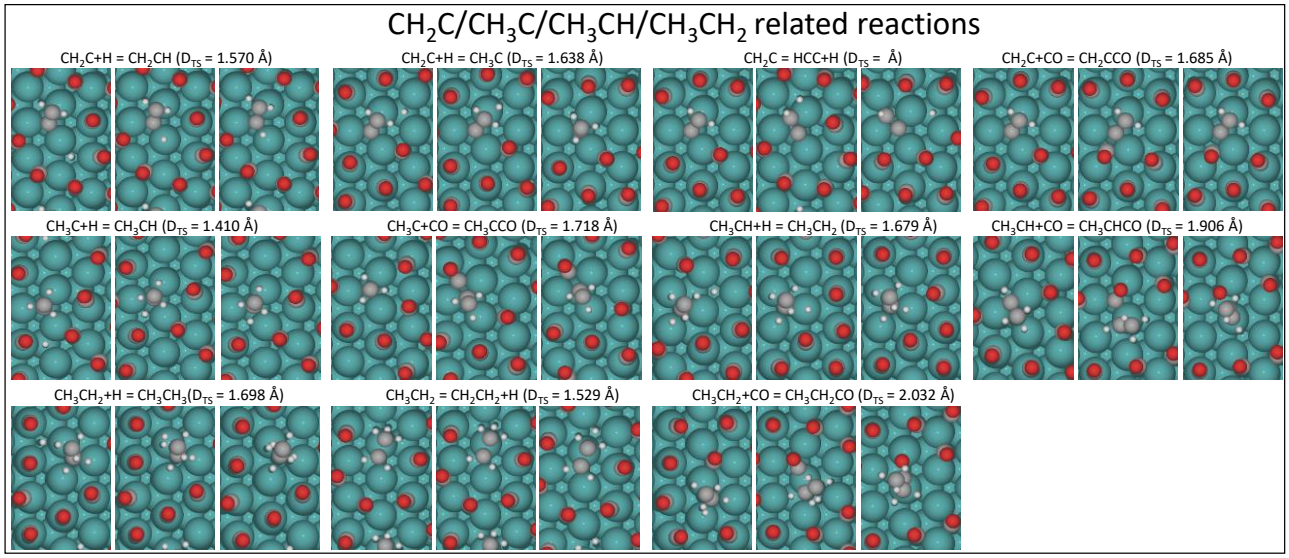

Figure S17. Surface structures of the initial (IS), transition (TS) and final (FS) states for the $CH_2C/CH_3C/CH_3CH/CH_3CH_2$ related reactions at CO pre-saturation coverage. Elementary reactions along with the forming/dissociating C-X bond length (D_{TS}) in the transition states are given.

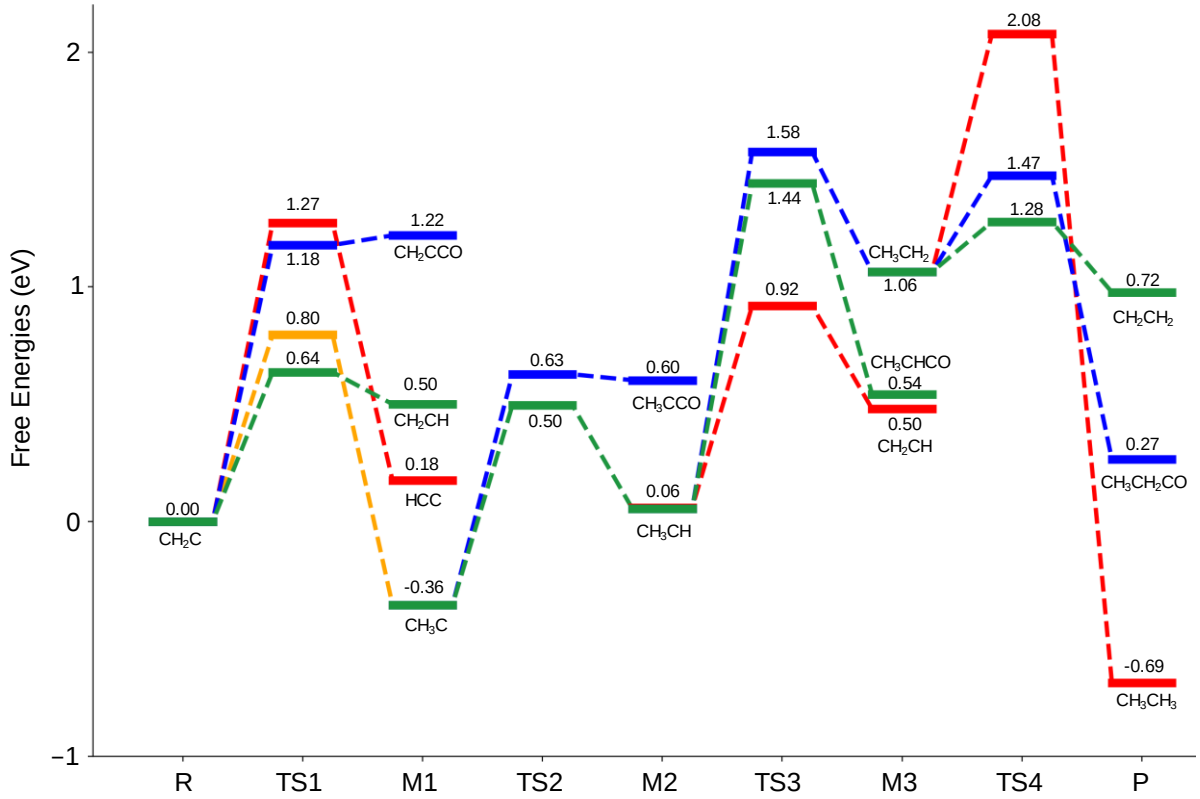

Figure S18. Gibbs free energy profiles of CH_2C and CH_3C development on the basis of gaseous H_2 at CO pre-saturation coverage

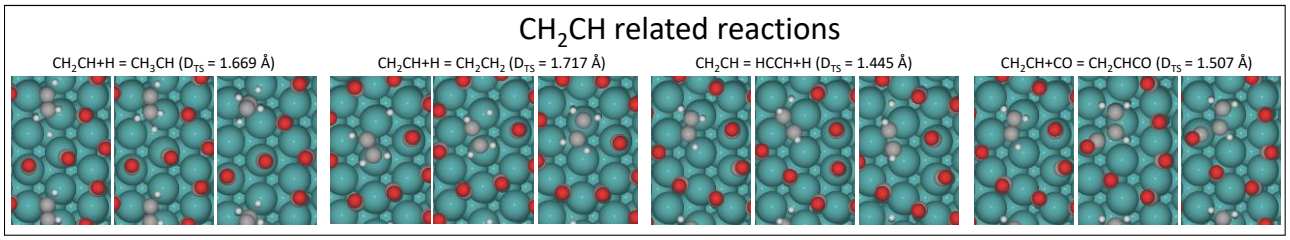

Figure S19. Surface structures of the initial (IS), transition (TS) and final (FS) states for the CH_2CH related reactions at CO pre-saturation coverage. Elementary reactions along with the forming/dissociating C-X bond length (D_{TS}) in the transition states are given.

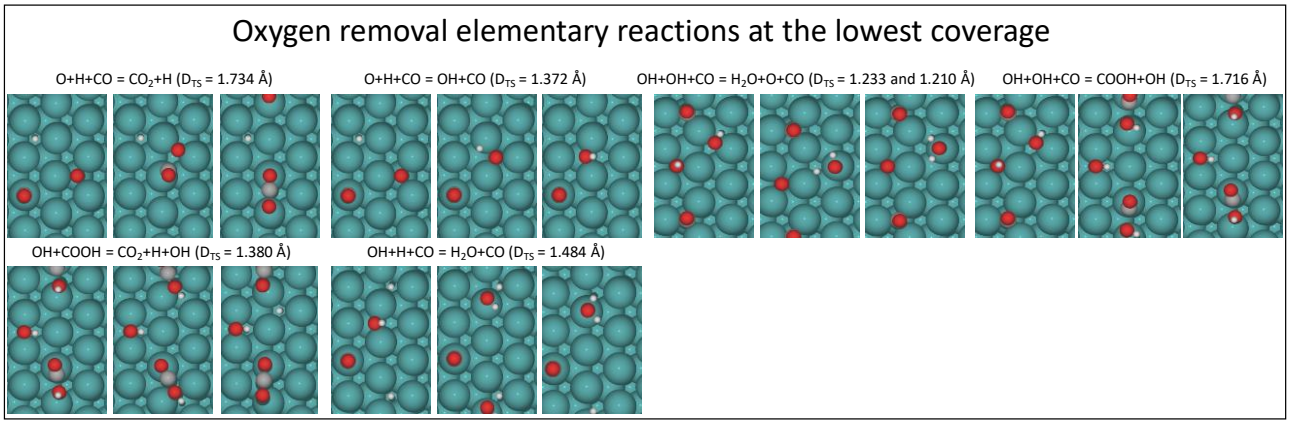

Figure S20. Surface structures of the initial (IS), transition (TS) and final (FS) states for the elementary reactions involved in oxygen removal at the lowest coverage. Elementary reactions along with the forming/dissociating C-X bond length (D_{TS}) in the transition states are given.

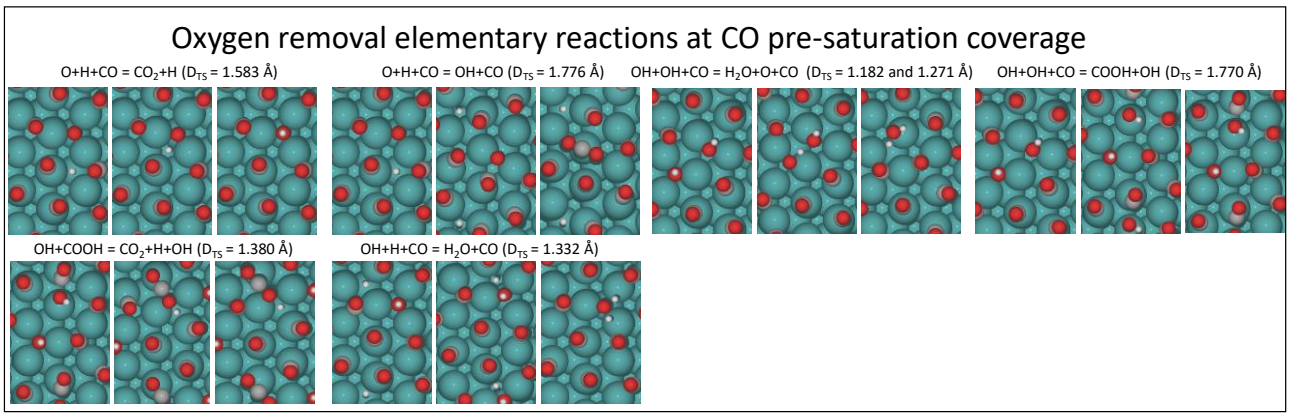

Figure S21. Surface structures of the initial (IS), transition (TS) and final (FS) states for the elementary reactions involved in oxygen removal at the highest CO coverage. Elementary reactions along with the forming/dissociating C-X bond length (D_{TS}) in the transition states are given.

Table S3. The reaction energies (eV) of RDS of our proposed mechanism at different CO/H coverage.

n_{CO}	n_H	$E_r(CH_3CO \rightarrow CH_3C+O)$	$E_r(CH_3+CO \rightarrow CH_3CO)$
1	4	−0.67	0.30
1	0	−0.84	0.62
2	2	−0.56	0.29
2	0	−0.77	0.70
3	0	−0.66	0.21
6	0	−0.84	−0.05

At given CO pre-coverage (0.11 and 0.22 ML, respectively), it is found that the reaction of $CH_3CO \rightarrow CH_3C+O$ become more exergonic (−0.67 vs. −0.84 eV; and −0.56 vs. −0.77 eV, respectively) with the decrease of H coverage, while totally opposite trend is found for the reaction of $CH_3+CO \rightarrow CH_3CO$, i.e., it becomes more endergonic (0.30 vs. 0.62 eV and 0.29 vs. 0.70 eV, respectively) with the decrease of H coverage. This indicated that decreasing H coverage can gradually promote $CH_3CO \rightarrow CH_3C+O$, while inhibit $CH_3+CO \rightarrow CH_3CO$.

With the increase of CO pre-coverage (0.11, 0.22 and 0.33 ML) the reaction of $CH_3CO \rightarrow CH_3C+O$ become less exergonic (−0.84; −0.77; and −0.66 eV, respectively), while the reaction of $CH_3+CO \rightarrow CH_3CO$ is endergonic at 0.11, 0.22 and 0.33 ML CO pre-coverage (0.62, 0.70 and 0.21 eV, respectively). At the highest CO pre-coverage (0.67 ML), the reaction of $CH_3CO \rightarrow CH_3C+O$ is exergonic by 0.84 eV, and the reaction of $CH_3+CO \rightarrow CH_3CO$ becomes exergonic by 0.05 eV. This abnormal change is due to the more sensitive lateral interaction of CO molecules at high coverage than at low coverage.

Micro-kinetics analysis

Along with the computed energetics of the formation of the first and second C-C bonds, their subsequent development, the formation of CH_3CHO, CH_3CH_2OH, CH_2CH, and HCCH, and the removal of surface oxygen, we also performed micro-kinetics analysis to estimate the reaction rate under the consideration of concentrations of surface species and surface adsorption sites for adsorption. Using a common energy reference (H_2, CO, and H_2O or CO_2), we summarized all rate-determining steps (RDS) of CH_4, C2 chain initiator, CH_3CHO, CH_3CH_2OH, CH_2CH_2, HCCH and possible C3 chain initiator at the lowest coverage (Figure S22) and at CO pre-saturation coverage (Figure S23). Full energy profiles are divided by three stages: CO activation, first C-C bond formation, and second C-C bond formation. Our proposed chain growth mechanism was consecutively plotted, and the highest point of the energy profile of the formation of CH_3CHO, CH_3CH_2OH, CH_2CH_2, and HCCH were marked with red stars. Micro-kinetics analysis of the removal of surface oxygen also was done and discussed below.

At the lowest coverage (Figure S22), the formation of CH_4 and the first C-C coupling share the same intermediate CH_2, and they are competitive. Next, the formation of CH_3CHO and CH_3CH_2OH share the same intermediate (CH_3CO) with the formation of C2 initiator. Similarly, the formation of CH_2CH_2 and HCCH formation will be competitive with the formation of C3 initiator.

The first C-C bond formation at the lowest coverage has the RDS of $CH_3CO \rightarrow CH_3C+O$ with an apparent barrier of −0.23 eV, and this step is irreversible because of its strong exergonicity (−1.93 eV). Correcting these energies with CO, H_2 and H_2O as references, the apparent barrier of CH_4 formation is higher than that of the formation of C2 initiator (0.11 vs. −0.23 eV), while the formation of CH_3CHO and CH_3CH_2OH has close apparent barrier with the formation of C2 initiator (−0.28 vs. −0.23 eV). The second C-C coupling, $CH_3CH+HCO \rightarrow CH_3CHCHO$, has an apparent barrier of −0.93 eV and is exergonic by 1.52 eV. The highest point of the formation of CH_2CH_2 and HCCH is −1.06 and −1.11 eV in their own free energy profiles, respectively. These corrected apparent barriers will be used to obtain rate constant of their formation rate.

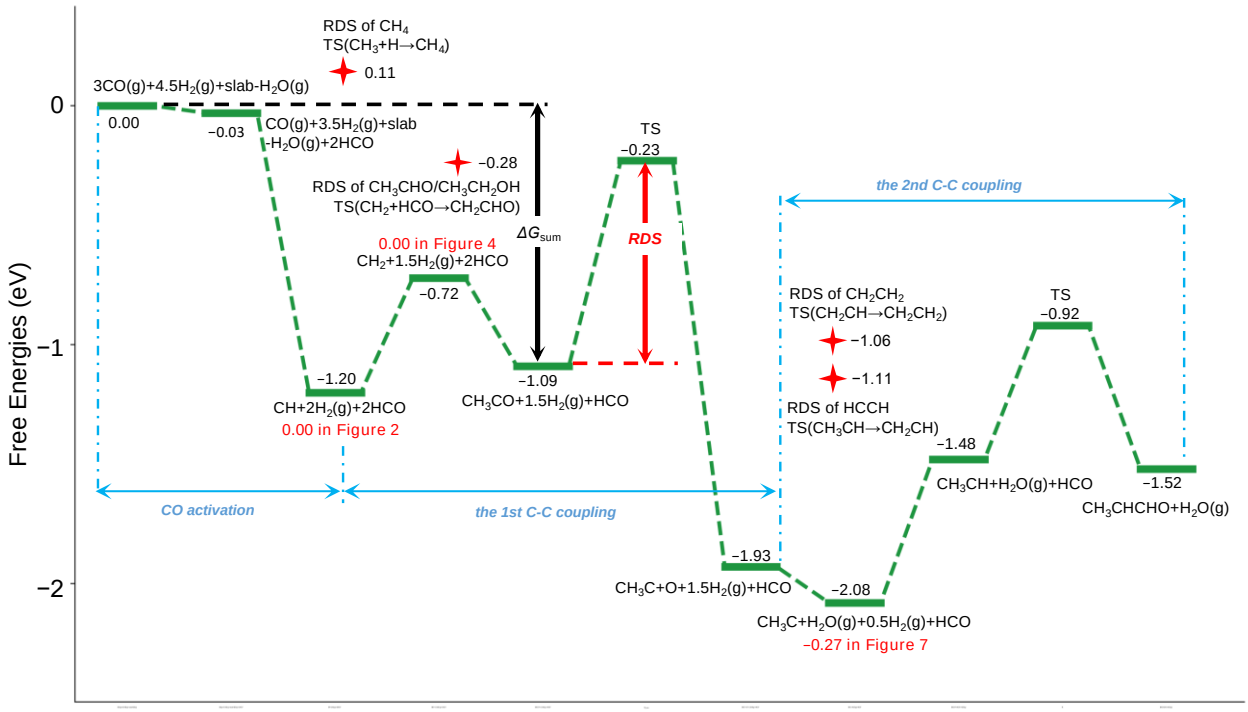

Figure S22. Full scheme of micro-kinetics analysis at the lowest coverage.

At CO pre-saturation coverage with CO, H_2 and CO_2 as references (Figure S23), the first C-C bond formation has the RDS of CH_3+6CO → CH_3CO+5CO with an apparent barrier of −2.59 eV and is exergonic by 4.06 eV. The highest point of the first C-C bond formation is 0.53 eV lower than that of CO activation (CO self-promoting hydrogenation route[4]). The second C-C coupling of CH_3CH+CO → CH_3CHCO has an apparent barrier of −4.21 eV and is exergonic by 5.11 eV. In addition, the formation of CH_4, CH_3CHO, CH_3CH_2OH, CH_2CH_2, and HCCH has an apparent barrier of −2.75, −2.56, −2.56, −4.08, and −4.67 eV, respectively.

Since the formation of CH_4, CH_3CHO, and CH_3CH_2OH occurs before the first C-O bond dissociation, they will compete with the formation of C2 initiator, while the formation of CH_2CH_2 and HCCH takes place after the first C-O bond dissociation, they will be competitive with the formation of the C3 initiator. Consequently, the formation of C2 initiator is not favored kinetically compared with that of methane (−2.75 vs. −2.59 eV), however, high CO coverage inhibits H_2 adsorption and the subsequent hydrogenation steps, the formation of C2 initiator can be promoted at CO pre-saturation coverage as discussed below.

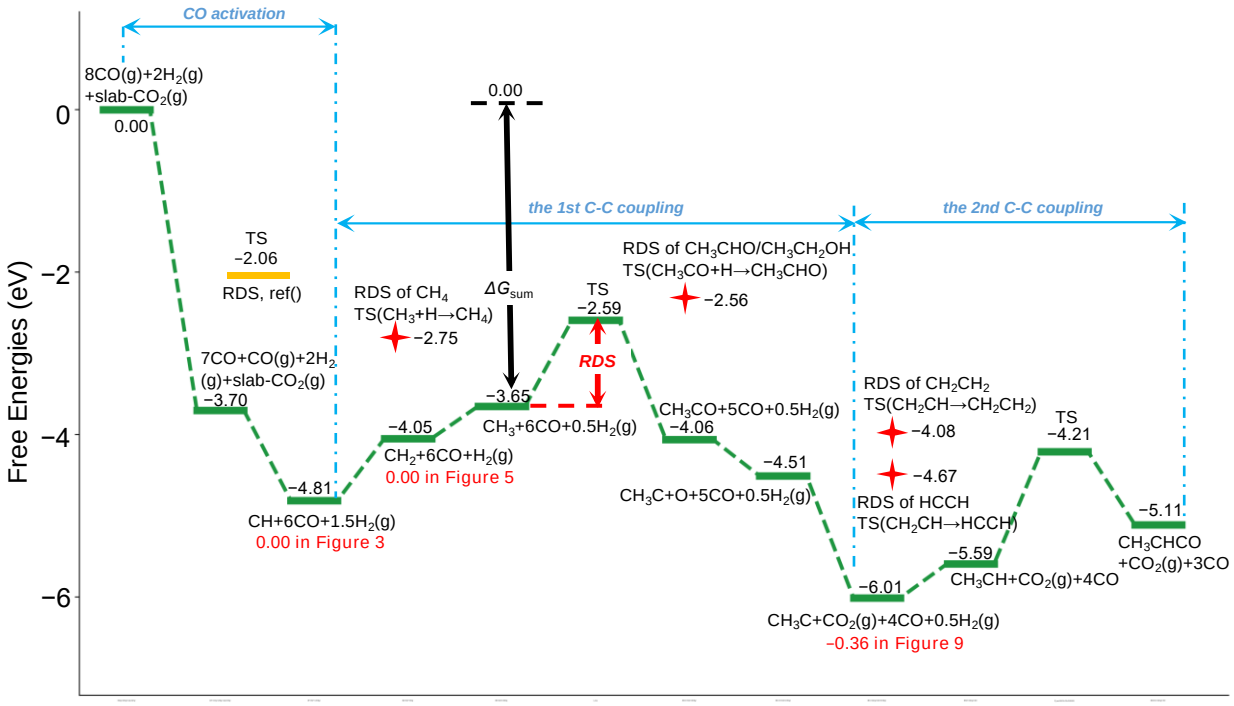

Figure S23. The full scheme of micro-kinetics analysis at CO pre-saturation coverage.

On the basis of our thermodynamics results, a complete reaction network starting from gaseous CO and H_2 can be constructed by the following elementary reactions(Table S4). To embody lateral interactions, the adsorption of C1 species and C2 species is thought respectively to occupy one or two sites.

Table S4. The elementary steps of chain growth process, CH_4, CH_3CHO, CH_3CH_2OH, CH_2CH_2, and HCCH formation

Reaction at lowest coverage(RL)		Reaction at CO pre-saturation coverage (RH)	
CO activation			
CO(g)+*=CO*	RL1	CO(g)+*=CO*	RH1
H_2(g)+2*=2H*	RL2	H_2(g)+2*=2H*	RH2
CO*+H*=HCO*	RL3		
1st C-C coupling			
C*+H*=CH*+*	RL4	C*+H*+6CO*=CH*+*+6CO*	RH3
CH*+H*=CH_2*+*	RL5	CH*+H*+6CO*=CH_2*+*+6CO*	RH4
CH_2*+HCO*=CH_2CHO*+*	RL6	CH_2*+6CO*+H*=CH_3*+6CO*+*	RH5
CH_2CHO*+*=CH_2CO*+H*	RL7	CH_3*+6CO*=CH_3CO*+5CO*+*	RH6
CH_2CO*+H*=CH_3CO*	RL8	CH_3CO*+*+5CO*=CH_3C*+O*+5CO*	RH7
CH_3CO*+*=CH_3C*+O*	RL9		
2nd C-C coupling			
CH_3C*+H*=CH_3CH*+*	RL10	CH_3C*+H*+5CO*=CH_3CH*+*+5CO*	RH8
CH_3CH*+HCO*=CH_3CHCHO*+*	RL11	CH_3CH*+5CO*=CH_3CHCO*+*+4CO*	RH9
removal of surface O			
2O*+2H*=2OH*+2*	RL12	2O*+5CO*+2H*=2OH*+5CO*+2*	RH10
2OH*=H_2O*+O*	RL13	2OH*+5CO*=H_2O*+O*+65O*	RH11
H_2O*=H_2O(g)+*	RL14	H_2O*+5CO*+O*=H_2O(g)+5CO*+O*	RH12
O*+CO*=CO_2*+*	RL15	O*+6CO*=CO_2*+6CO*	RH13
CO_2*=CO_2(g)	RL16	CO_2*+6CO*=CO_2(g)+*+6CO*	RH14
methane formation			
CH_2*+H*=CH_3*+*	RL17	CH_2*+H*+6CO*=CH_3*+*+6CO*	RH15
CH_3*+H*=CH_4*+*	RL18	CH_3*+H*+6CO*=CH_4*+*+6CO*	RH16
CH_4*=CH_4(g)	RL19	CH_4*+6CO*=CH_4(g)+6CO*	RH17
CH_3CHO and CH_3CH_2OH formation			
CH_2CHO*+H*=CH_3CHO*+*	RL20	CH_3CO*+H*+5CO*=CH_3CHO*+*+5CO*	RH18
CH_3CHO*=CH_3CHO(g)+*	RL21	CH_3CHO*+5CO*=CH_3CHO(g)+5CO*	RH19
CH_3CHO*+H*=CH_3CH_2O*+*	RL22	CH_3CHO*+5CO*+H*=CH_3CH_2O*+*+5CO*	RH20
CH_3CH_2O*+H*=CH_3CH_2OH*+*	RL23	CH_3CH_2O*+H*+5CO*=CH_3CH_2OH*+*+5CO*	RH21
CH_3CH_2OH*=CH_3CH_2OH(g)+*	RL24	CH_3CH_2OH*+5CO*=CH_3CH_2OH(g)+5CO*	RH22
CH_2CH_2 and HCCH formation			
CH_3C*+H*=CH_3CH*+*	RL25	CH_3C*+H*+5CO*=CH_3CH*+*+5CO*	RH23
CH_3CH*+*=CH_2CH*+H*	RL26	CH_3CH*+*+5CO*=CH_2CH*+H*+5CO*	RH24
CH_2CH*+H*=CH_2CH_2*+*	RL27	CH_2CH*+H*+5CO*=CH_2CH_2*+*+5CO*	RH25
CH_2CH_2*=CH_2CH_2(g)+*	RL28	CH_2CH_2*+5CO*=CH_2CH_2(g)+*+5CO*	RH26
CH_2CH*+*=HCCH*+H*	RL29	CH_2CH*+*+5CO*=HCCH*+H*+5CO*	RH27

Since surface O can be removed as H_2O(g) and CO_2(g) at the lowest and CO pre-saturation coverage, respectively, we used CO and H_2 as a common energy reference. On the basis of material conservation principle under the proposed reaction conditions (423 K, 30 atm, and $p_{H2}/p_{CO}/p_{CH4}/p_{CO2}/p_{H2O}$ = 10/5/2/2/1), the energy reference of starting point (CH*) can be corrected to −1.20 eV and −4.81 eV at the lowest and CO pre-saturation coverage, respectively.

Starting from CH* and CH*+6CO*, the highest point of the full energy profile of the first C-C bond formation, the transition state of the breaking of C-O bond in CH_3CO* and the coupling of CH_3 + CO which represents the rate-determining step (RDS), should determine the rate of the first C-C bond formation at the lowest and CO pre-saturation coverage, respectively. In our simplified micro-kinetics model, all other steps except RDS are assumed to have quasi-equilibrium. Therefore, the rate of the first C-C coupling reaction can be expressed by Eq. S1 at the lowest coverage (RL) and Eq. S2 at CO pre-saturation coverage (RH):

$$r_{RL,\,C2} = k^{+}_{RL9}\ [CH_3CO^*][^*] \qquad \text{Eq. S1}$$

$$r_{RH,\,C2} = k^{+}_{RH6}\ [CH_3^*][CO^*]^6 \qquad \text{Eq. S2}$$

wherein, k^{+}_{RL9} and k^{+}_{RH6} are the respective forward rate constant of RL9 and RH6 (Table S4), $r_{RL, C2}$ and $r_{RH, C2}$ are the respective rate of the first C-C coupling at the lowest and CO pre-saturation coverage, and the concentration of surface species (also surface free sites), [X], represents the number of the adsorbed X per square meter (/m^2).

Because of the proposed quasi-equilibrium, an equilibrium constant of RL8 can be expressed by Eq. S3:

$$K_{RL8} = ([CH_3CO^*][^*])/([CH_2CO^*][H]^*) \quad \text{Eq. S3}$$

Wherein, for a given reaction RLn or RHn, the equilibrium constant should be K_{RLn} or K_{RHn}

So,

$$[CH_3CO^*][^*] = K_{RL8}[CH_2CO^*][H^*] \quad \text{Eq. S4}$$

Similarly,

$$[CH_2CO^*][H^*] = K_{RL7}[CH_2CHO^*][^*] \quad \text{Eq. S5}$$

$$[CH_2CHO^*][^*] = K_{RL6}[CH_2^*][HCO^*] \quad \text{Eq. S6}$$

Then,

$$[CH_3CO^*][^*] = K_{RL8}K_{RL7}K_{RL6}K_{RL5}K_{RL4}K_{RL3}K_{RL2}K_{RL1}\cdots[CO(g)]^2[H_2(g)]^{2.5}[H_2O(g)]^{-1}[^*]^2 \quad \text{Eq. S7}$$

Substituting Eq. S7 to Eq. S1, we can get Eq. S8

$$r_{RL, C2} = k^{+}_{RL9}K_{RL8}K_{RL7}K_{RL6}K_{RL5}K_{RL4}K_{RL3}K_{RL2}K_{RL1}\cdots[CO(g)]^2[H_2(g)]^{2.5}[H_2O(g)]^{-1}[^*]^2 \quad \text{Eq. S8}$$

According to the Eyring equation of

$$k = (\kappa k_B T/h)\exp(-\Delta G^{\neq}/RT) \quad \text{Eq. S9}$$

Wherein, k is the rate constant, $\Delta G^{\neq}$ is the Gibbs energy of activation, κ is the transmission coefficient, k_B is the Boltzmann constant, T is the temperature and h is the Planck constant.

For an equilibrium reaction,

$$\Delta G_r = -RT\ln K_r \quad \text{Eq. S10}$$

Wherein, ΔG_r and K_r is respective Gibbs free energy and equilibrium constant of reaction.

Substituting Eq. S9 and Eq. S10 to Eq. S8, we can get

$$r_{RL, C2} = (\kappa k_B T/h)\exp[-(\Delta G_{RL9}^{\neq} + \Delta G_{sum,\ before\ RL9})/RT][CO(g)]^2[H_2(g)]^{2.5}[H_2O(g)]^{-1}[^*]^3 \quad \text{Eq. S11}$$

Wherein, $\Delta G_{sum,\ before\ RDS}$ is the sum of Gibbs free energies of all the elementary reactions before rate-determining step (RDS) and $\Delta G_{RL9}^{\neq}$ is the barrier of the RDS.

Analogy to that at the lowest coverage, we also can convert Eq. S2 to Eq. S12 on the basis of gaseous CO, H_2 and CO_2 at CO pre-saturation coverage

$$r_{RH, C2} = (\kappa k_B T/h)\exp[-(\Delta G_{RH6}^{\neq} + \Delta G_{sum,\ before\ RH6})/RT][CO(g)]^8[H_2(g)]^{1.5}[CO_2(g)]^{-1}[^*]^7 \quad \text{Eq. S12}$$

Similarly, the rate of the second C-C formation can be determined by RL11 and RH9 respectively, and the rate equation can finally be expressed by

$r_{RL,\ C3} = (\kappa k_B T/h)\exp[-(\Delta G_{RL11}^{\neq} + \Delta G_{sum,\ before\ RL11})/RT][CO(g)]^3[H_2(g)]^{4.5}[H_2O(g)]^{-2}[*]^3$ Eq. S13

$r_{RH,\ C3} = (\kappa k_B T/h)\exp[-(\Delta G_{RH9}^{\neq} + \Delta G_{sum,\ before\ RH9})/RT][CO(g)]^9[H_2(g)]^2[CO_2(g)]^{-2}[*]^7$ Eq. S14

The formation of CH_4 has the RDS of the hydrogenation of CH_3 (Table S4, RL18 at the lowest coverage and RH16 at CO pre-saturation coverage). At the lowest coverage, the formation of CH_3CHO and CH_3CH_2OH has the same RDS of CH_2+HCO → CH_2CHO) (RL6) and the formation of CH_2CH_2 and HCCH has the RDS of CH_2CH*+H* → CH_2CH_2*+* (RL27) and of CH_3CH*+* → CH_2CH*+H* (RL26), respectively. At CO pre-saturation coverage, the formation of CH_3CHO and CH_3CH_2OH has the same RDS of the hydrogenation of CH_3CO into CH_3CHO (RH18) and the formation of CH_2CH_2 and HCCH has the RDS of CH_2CH*+H*+5CO* → CH_2CH_2*+*+5CO* (RH25) and of CH_2CH*+*+5CO* → HCCH*+H*+5CO*(RH27), respectively. Therefore, we can express the rate of CH_4, CH_3CHO, CH_3CH_2OH, CH_2CH_2, and HCCH formation in the following:

At the lowest coverage,

$r_{RL,\ CH4} = k_{RL18}^{+}\ [CH_3*][H*]$ Eq. S15

$r_{RL,\ CH3CH2OH/CH3CHO} = k_{RL6}^{+}\ [CH_2*][HCO*]$ Eq. S16

$r_{RL,\ CH2CH2} = k_{RL27}^{+}\ [CH_2CH*][H*]$ Eq. S17

$r_{RL,\ HCCH} = k_{RL26}^{+}\ [CH_3CH*][*]$ Eq. S18

$r_{RL,\ H2O} = k_{RL12}^{+}\ [O*]^2[H*]^2$ Eq. S19

$r_{RL,\ CO2} = k_{RL15}^{+}\ [O*][CO*]$ Eq. S20

At CO pre-saturation coverage,

$r_{RH,\ CH4} = k_{RH16}^{+}\ [CH_3*][H*][CO*]^6$ Eq. S21

$r_{RH,\ CH3CH2OH/CH3CHO} = k_{RH18}^{+}\ [CH_3CO*][H*][CO*]^5$ Eq. S22

$r_{RH,\ CH2CH2} = k_{RH25}^{+}\ [CH_2CH*][H*][CO*]^5$ Eq. S23

$r_{RH,\ HCCH} = k_{RH27}^{+}\ [CH_2CH*][*][CO*]^5$ Eq. S24

$r_{RH,H2O} = k_{RH10}^{+}\ [O*]^2[H*]^2[CO*]^5$ Eq. S25

$r_{RH,CO2} = k_{RH13}^{+}\ [O*][CO*]^6$ Eq. S26

Wherein, k_{RLn}^{+} or k_{RHn}^{+} is respectively the forward rate constant of reaction RLn or RHn. r is the rate of the corresponding elementary reaction.

Similar with the chain growth process, we analyzed the rate of the formation of CH_4, CH_3CHO, CH_3CH_2OH, CH_2CH_2, HCCH, H_2O, and CO_2 by assuming all the other steps except RDS are quasi-equilibrium. Then, equations S15-S26 can be expressed by the following:

At the lowest coverage (RL),

$R_{RL,\ CH4} = (\kappa k_B T/h)\exp[-(\Delta G_{RL9}^{\neq} + \Delta G_{sum,\ before\ RL18})/RT][CO(g)][H_2(g)]^3[H_2O(g)]^{-1}[*]^2$ Eq. S27

$R_{RL,\ CH3CH2OH/CH3CHO} = (\kappa k_B T/h)\exp[-(\Delta G_{RL6}^{\neq} + \Delta G_{sum,\ before\ RL6})/RT][CO(g)]^2[H_2(g)]^{2.5}[H_2O(g)]^{-1}[*]^2$ Eq. S28

$R_{RL,\ CH2CH2} = (\kappa k_B T/h)\exp[-(\Delta G_{RL27}^{\neq} + \Delta G_{sum,\ before\ RL27})/RT][CO(g)]^2[H_2(g)]^4[H_2O(g)]^{-2}[*]^3$ Eq. S29

$R_{RL,HCCH} = (\kappa k_B T/h)\exp[-(\Delta G_{RL26}^{\neq} + \Delta G_{sum,\ before\ RL26})/RT][CO(g)]^2[H_2(g)]^4[H_2O(g)]^{-2}[*]^3$ Eq. S30

$R_{RL,H2O} = (\kappa k_B T/h)\exp[-(\Delta G_{RL12}^{\neq} + \Delta G_{sum,\ before\ RL12})/RT][O*]^2[H_2(g)][*]^2$ Eq. S31

$R_{RL,CO2} = (\kappa k_B T/h)\exp[-(\Delta G_{RL15}^{\neq} + \Delta G_{sum,\ before\ RL15})/RT][O*][CO(g)][*]$ Eq. S32

At CO pre-saturation coverage (RH),

$R_{RH,\ CH4} = (\kappa k_B T/h)\exp[-(\Delta G_{RH16}^{\neq} + \Delta G_{sum,\ before\ RH16})/RT][CO(g)]^8[H_2(g)]^2[CO_2(g)]^{-1}[*]^8$ Eq. S33

$R_{RH,\ CH3CH2OH/CH3CHO} = (\kappa k_B T/h)\exp[-(\Delta G_{RH18}^{\neq} + \Delta G_{sum,\ before\ RH18})/RT][CO(g)]^8[H_2(g)]^2[CO_2(g)]^{-1}[*]^8$ Eq. S34

$R_{RH,\ CH2CH2} = (\kappa k_B T/h)\exp[-(\Delta G_{RH25}^{\neq} + \Delta G_{sum,\ before\ RH25})/RT][CO(g)]^9[H_2(g)]^2[CO_2(g)]^{-2}[*]^8$ Eq. S35

$R_{RH,HCCH} = (\kappa k_B T/h)\exp[-(\Delta G_{RH27}^{\neq} + \Delta G_{sum,\ before\ RH27})/RT][CO(g)]^9[H_2(g)]^{1.5}[CO_2(g)]^{-2}[*]^8$ Eq. S36

$R_{RH,H2O} = (\kappa k_B T/h)\exp[-(\Delta G_{RH10}^{\neq} + \Delta G_{sum,\ before\ RH10})/RT][O*]^2[CO(g)]^5[H_2(g)][*]^9$ Eq. S37

$R_{RH,CO2} = (\kappa k_B T/h)\exp[-(\Delta G_{RH13}^{\neq} + \Delta G_{sum,\ before\ RH13})/RT][O*][CO(g)]^6[*]^7$ Eq. S38

The above discussion shows that the formation of CH_4, CH_3CHO, and CH_3CH_2OH is competitive with the first C-C bond formation, and the formation of CH_2CH_2 and HCCH is competitive with the second C-C bond formation at both lowest coverage and CO pre-saturation coverage.

We analyzed ratio of the rate constant, the ratio of the concentration of surface species, and the ratio of the reaction rate on the basis of our simplified micro-kinetic models. We assumed that the number of the sites of each slab is 7 (the maximum number of adsorbed CO is 7CO), the number of free sites [*] of each slab is 5 and 0, respectively, at the lowest coverage and CO pre-saturation coverage. At CO pre-saturation coverage, the site for H ($0.5H_2$) adsorption is not favorable thermodynamically and the probability of H adsorption is rather low under the proposed reaction conditions (423 K, 30 atm, and $p_{H2}/p_{CO}/p_{CH4}/p_{CO2}/p_{H2O}$ = 10/5/2/2/1).

For the removal of surface oxygen, only one surface oxygen is used in one slab. At the lowest coverage for one oxygen atom on the slab surface, stepwise addition of H atom has been used for the formation of H_2O, and addition of one CO molecule has been used for the formation for CO_2.

All concentrations of surface species (included surface free sites) are represented by the number per unit area (m^2) and all concentrations of gaseous species are represented by the number per unit volume (m^3). The results are shown in Table S5.

Table S5. A comparison between the reaction rate of chain growth and the reaction rate of products (CH_3CHO, CH_3CH_2OH, CH_2CH_2, and HCCH) on the basis of simplified micro-kinetics model.

products	Ratio of rate constant	Ratio of concentrations	Ratio of reaction rate
		At the lowest coverage	
$[CH_4]/[C2]$	9.03×10^{-5}	1.33×10^{5} ($[H_2(g)]^{0.5}[CO(g)]^{-1}[*]^{-1}$)	12.01
$[CH_3CHO]/[C2]$	3.93	1.14×10^{-18} ($[*]^{-1}$)	4.48×10^{-18}
$[CH_3CH_2OH]/[C2]$	3.93	1.14×10^{-18} ($[*]^{-1}$)	4.48×10^{-18}

$[CH_2CH_2]/[C3]$	46.26	8.75×10^{-40} ($[CO(g)]^{-1}[H_2(g)]^{-0.5}$)	4.05×10^{-38}
$[HCCH]/[C3]$	181.96	8.75×10^{-40} ($[CO(g)]^{-1}[H_2(g)]^{-0.5}$)	4.05×10^{-38}
$[H_2O]/[CO_2]$	1.46×10^{4}	3.07×10^{37}($[O^*][H_2(g)][^*][CO(g)]^{-1}$)	4.47×10^{41}
		CO pre-saturation coverage	
$[CH_4]/[C2]$	80.01	0 ($[H_2(g)]^{0.5}[^*]$)	0
$[CH_3CHO]/[C2]$	0.44	0 ($[H_2(g)]^{0.5}[^*]$)	0
$[CH_3CH_2OH]/[C2]$	0.44	0 ($[H_2(g)]^{0.5}[^*]$)	0
$[CH_2CH_2]/[C3]$	0.03	0 ($[^*]$)	0
$[HCCH]/[C3]$	2.96×10^{5}	0 ($[^*][H_2(g)]^{-0.5}$)	0
$[H_2O]/[CO_2]$	105.22	0 ($[O^*][H_2(g)][^*]^2[CO(g)]^{-1}$)	0

At the lowest coverage, the ratio of the rate constant term of the formation CH_4 and C2 chain initiator is 9.03×10^{-5} and the corresponding ratio of the concentration term is 1.33×10^{5}. As a result, the rate of the formation of methane is greater than that of the formation of C2 initiator (12.01 to 1). Next, the ratio of the formation of CH_3CHO and CH_3CH_2OH vs. C2 initiator is 3.93 to 1 on one hand, and one the other hand, the corresponding ratio of the concentration terms of surface species is 1.14×10^{-18}. Totally, the rate of the formation of CH_3CHO and CH_3CH_2OH is much smaller than that of the formation of C2 initiator (4.48×10^{-18} to 1). The reason for such huge rate difference comes from that fact that there are sufficient free sites for the dissociation reaction of RL9, which is the RDS of the formation of C2 initiator. Then, the rate of the formation of CH_2CH_2 and HCCH is also much smaller than that of the formation of C3 initiator (4.05×10^{-38} and 4.05×10^{-38} to 1), and this is because that the second C-C bond formation is more sensitive on the partial pressure of CO and H_2, as indicated by the ratio of the concentration term, $[CO(g)]^{-1}[H_2(g)]^{-0.5}$. Comparing all these ratios of the reaction rates, the formation of methane is more favored than that of the chain growth process at the lowest coverage.

At CO pre-saturation coverage, the ratio of the rate-constant of methane formation and the formation of C2 initiator is 80 to 1. On the basis of the ratio of the concentration term ($[H_2(g)]^{0.5}[^*]$), the formation of methane needs one free site to adsorb $0.5H_2(g)$. However, it is difficult to adsorb one H atom with adsorption-desorption equilibrium constant of 2.34×10^{-8} (as discussed in main text) and the probability of free sites on the surface is rather low (close to 0). Similar situations are found for the formation of CH_2CH_2, HCCH, CH_3CHO, and CH_3CH_2OH. Due to high requirements of H content, hydrogenation reaction is remarkably inhibited. Therefore, the chain growth process is more favored than the formation of CH_4, CH_3CHO, CH_3CH_2OH, CH_2CH_2, and HCCH, and this is because that the chain growth process (CO-insertion mechanism for the formation of C2 and C3 initiator) needs less free sites at CO pre-saturation coverage.

The removal of surface oxygen as H_2O and CO_2 is competitive at the lowest coverage and the CO pre-saturation coverage. At the lowest coverage, the ratio of the rate constant of the formation of H_2O and CO_2 is 1.46×10^{4} to 1, and the formation of H_2O is more favored not only by the kinetic term but also by the concentration term. As a result, the rate of H_2O formation will be much greater than that of CO_2 formation (4.47×10^{41} to 1). At CO pre-saturation coverage, CO_2 formation is much more favored than that of H_2O despite the more favored kinetic preference of H_2O formation, and this is because that H_2O formation is highly dependent on the availability of free sites for H_2 adsorption, which are very limited at CO pre-saturation coverage, as indicated by the ratio of

concentration terms of H_2O/CO_2 formation ($[O^*][H_2(g)][^*]^2[CO(g)]^{-1}$). Consequently, surface oxygen should be removed as CO_2 rather than as H_2O.

References

1 P. Zhao, Y. R. He, D. B. Cao, X. D. Wen, H. W. Xiang, Y. W. Li, J. G. Wang and H. J. Jiao, *Phys. Chem. Chem. Phys.,* 2015, **17**,19446-19456.

2 B. A. J. Lechner, X. F. Feng, P. J. Feibelman, J. I. Cerda and M. Salmeron, *J. Phys. Chem. B,* 2018, **122**, 649-656.

3 H. Pfnür, P. Feulner and D. Menzel, *J. Chem. Phys.,* 1983, **79**, 4613-4623.

4 P. Zhao, Y. R. He, D. B. Cao, H. W. Xiang, H. J. Jiao, Y. Yang, Y. W. Li and X. D. Wen, *J. Phys. Chem. C ,* 2019, **123**, 6508-6515.